Supporting Online Material for

Mechanisms of Proton Conduction and Gating by Influenza M2 Proton Channels From Solid-State NMR

Fanghao Hu, Wenbin Luo, and Mei Hong*

Department of Chemistry, Iowa State University, Ames, IA 50011

* To whom correspondence should be addressed. Email: mhong@iastate.edu

Materials and Methods

Membrane sample preparation

The transmembrane domain (residues 22-46, SSDPLVVAAS IIGILHLILW ILDRL) of the M2 protein of the influenza A Udorn strain was synthesized by PrimmBiotech (Cambridge, MA) using Fmoc solid-phase peptide synthesis protocols and was purified to >95% purity. The peptide used in this study was ^{13}C, ^{15}N-labeled at Gly34, His37 and Ile42. Fmoc-U-^{13}C, ^{15}N-His-trityl-OH was purchased from Sigma-Aldrich, and Fmoc protection of U-^{13}C, ^{15}N-labeled Gly and Ile were carried out in-house.

All phospholipids and cholesterol were purchased from Avanti Polar Lipids. A virus-envelope-mimetic membrane mixture including DPPC, DPPE, egg sphingomyelin (SPM) and cholesterol (Chol) (*1*) was used to reconstitute M2TM. This membrane mixture resembles the virus-envelope lipid composition, and gives higher-resolution protein spectra than model phosphocholine membranes. More importantly, the virus-mimetic membrane immobilizes the M2TM backbone at ambient temperature, in contrast to model lipid membranes, thus enabling sidechain dynamics to be extracted (*1-3*). To prepare the viral membrane, we dissolved sphingomyelin in a chloroform/methanol (5:1) solution and mixed it with DPPC, DPPE and cholesterol in chloroform at a molar ratio of SPM:DPPC:DPPE:Chol = 28:21:21:30. The solution was dried under a stream of nitrogen gas, suspended in cyclohexane and lyophilized. The dry lipid powder was resuspended in 1 mL buffer solution of defined pH, votexed, and free-thawed eight times to create uniform lipid vesicles. M2TM powder was codissolved with octyl-β-D-glucopyranoside (OG) in 1 mL of the buffer at an OG concentration of 20 mg/mL. The solution was then mixed with 1 mL lipid vesicle solution, votexed for 2 hours and dialyzed with a 3.5-kDa molecular weight cutoff against 1 L buffer at 4°C for 3 days with buffer changes every 8-12 hours to remove the detergent. The protein-lipid precipitate usually appeared after one day. The proteoliposome solution was centrifuged at 150,000g and 6 °C for 4 hours to yield a membrane pellet with a hydration level of ~40 wt%. The final protein : lipid molar ratio was 1 : 15. The pellet was packed into 4 mm MAS rotors for solid-state NMR experiments.

Four membrane samples at different pH were prepared for this study. A pH 8.5 sample was prepared in a Tris buffer containing 10 mM Tris, 1 mM EDTA, and 0.1 mM NaN_3. A pH 6.0 sample was prepared using a Bis-Tris buffer (10 mM Bis-Tris, 1 mM EDTA, and 0.1 mM NaN_3).

A pH 4.5 and pH 5.2 sample were prepared using a citrate buffer containing 10 mM citric acid/sodium citrate, 1 mM EDTA, and 0.1 mM NaN_3.

Solid-state NMR experiments

Solid-state NMR experiments were carried out on a Bruker DSX-400 MHz spectrometer at 9.4 Tesla and an AVANCE 600 MHz spectrometer at 14.1 Tesla (Karlsruhe, Germany). Magic-angle-spinning (MAS) probes with 4-mm diameter spinners were used. Typical radiofrequency (rf) pulse lengths were 5 μs for ^{13}C, 6-7 μs for ^{15}N and 3.5-4.0 μs for ^{1}H. ^{13}C chemical shifts were referenced to the α-Gly ^{13}CO signal at 176.49 ppm on the TMS scale, and ^{15}N chemical shifts were referenced to the ^{15}N signal of N-acetyl-valine at 122.0 ppm on the liquid ammonia scale.

^{13}C and ^{15}N chemical shifts were measured from two-dimensional ^{13}C-^{13}C and ^{13}C-^{15}N correlation experiments. The ^{13}C-^{13}C 2D experiments used a ^{1}H-driven ^{13}C spin diffusion pulse sequence with 40-60 ms DARR (*4*) mixing periods. The spectra were measured at 273 K under 7-10 kHz MAS. 2D ^{15}N-^{13}C correlation spectra were measured using a REDOR-based pulse sequence for ^{13}C-^{15}N coherence transfer (*5*). The experiments were conducted at 273 K and 243 K under 7-10 kHz MAS. A typical ^{13}C-^{15}N recoupling time of 0.6 ms was used to obtain one-bond ^{15}N-^{13}C cross peaks.

2D ^{15}N-detected ^{1}H spin diffusion experiments were used to detect His37-water cross peaks. The ^{1}H evolution period did not involve homonuclear decoupling, thus only the ^{1}H signals of mobile species such as water and lipids could survive. A short ^{1}H spin diffusion period of 50 μs followed the evolution time to allow water-His37 polarization transfer. A 1 ms ^{1}H-^{15}N Hartman-Hahn cross-polarization (CP) contact time established the ^{15}N magnetization. The spectra were measured at 303 K under 4.0 and 4.5 kHz MAS.

Two-dimensional ^{15}N-^{1}H and ^{13}C-^{1}H dipolar-chemical-shift (DIPSHIFT) correlation experiments (*6*) were used to measure N-H and C-H bond lengths at low temperature and molecular motion at high temperature. For the bond length measurements, the experiments were carried out under 4.3 or 5.0 kHz MAS at 243 K, at which both the protein backbone and sidechains were frozen. For the dynamics measurements, the DIPSHIFT experiments were carried out at 308 K and 303 K. The indirect dimension of the 2D experiment used either FSLG (*7*) or MREV-8 (*8*) sequences to decouple the ^{1}H-^{1}H dipolar interaction. The t_1 time-domain data

were fitted to obtain the apparent couplings, which were then divided by the scaling factor of the homonuclear decoupling sequence, which was 0.577 for FSLG and 0.47 for MREV-8, to obtain the true couplings. For ^{15}N-^{1}H dipolar couplings, the coupling-doubled version of the DIPSHIFT experiment (*9*) was used to enhance the accuracy of the coupling measurement.

To extract motional order parameters from DIPSHIFT data, both the homonuclear decoupling scaling factor and the rigid-limit coupling value contain uncertainties that may affect the order parameter values. To calibrate these effects, we measured the product of the scaling factor and the rigid-limit coupling using the crystalline model peptide formyl-Met-Leu-Phe (f-MLF) (*10*). Based on the theoretical scaling factors of FSLG and MERV-8, we obtained apparent rigid-limit values of 11.3 kHz for N-H and 22.7 kHz for Cα-Hα dipolar couplings. Using these values gave reasonable backbone order parameters of 0.95-1.00 for f-MLF. Therefore, we used these scaling factors and rigid-limit values in extracting His37 order parameters.

Backbone-sidechain distances that constrain the His37 χ_1 and χ_2 torsion angles were measured using ^{13}C{^{15}N} REDOR experiments that selectively irradiate the spins of interest (*11*). The ^{13}C-detected and ^{15}N-dephased experiment is denoted as ^{13}C{^{15}N}) REDOR. The pulse sequence used a selective Gaussian 180° pulse on both the ^{13}C and ^{15}N channels. The control experiment (S_0) did not have further ^{15}N pulses, while the dephasing experiment (S) contained multiple ^{15}N inversion pulses spaced half a rotor period apart. The ^{15}N inversion pulses used the composite pulse 90°180°90° to reduce the effects of pulse imperfection (*12*). For Cα-Nδ1 and Cδ2-Nα distance measurements, the experiments were carried out at 233 K where all sidechain motions were frozen, and MAS frequencies of 5.3, 7.0 and 8.0 kHz were used. The ^{13}C and ^{15}N Gaussian 180°-pulse lengths ranged from 1.125 to 2.0 ms, and the ^{15}N hard 90° pulse length was 7 μs. To characterize imidazole motion at ambient temperature, the Cγ-Nδ1 dipolar coupling was measured at 303 K under 7 kHz MAS, with a Gaussian 180°-pulse of 2 ms for ^{13}C and 1.14 ms for ^{15}N.

Data Analysis

Simulations of ^{13}C{^{15}N} REDOR distances to constrain the His37 rotameric structure

Distance fitting for the Cα to sidechain ^{15}N REDOR data took into account 1) the low amount of lipid natural-abundance ^{13}C intensities that overlapped with the His37 Cα peak, and 2)

10% correction for pulse imperfection at long mixing times (*12*). The percent of lipid intensities at the Cα peak was obtained by measuring the minimum S/S_0 ratio of the Cα peak when dephased by its directly bonded amide ^{15}N. The spectra were shown in **Fig. S2**. The percent of lipid intensities was about 30% at both pH 4.5 and pH 8.5.

Selective irradiation of the Nδ1 peak was required for measuring the Cα-Nδ1 distance. For the pH 8.5 sample, the 250-ppm peak is a superposition of 70% Nδ1 of the τ-tautomer and 30% Nε2 of the π-tautomer. However, the Cα-Nε2 distance is almost invariant (4.4 – 4.6 Å) between different rotamers and also much longer than the Cα-Nδ1 distance (3.2 – 3.9 Å). Thus, the Cα-Nδ1 REDOR data was primarily determined by the 70% Cα-Nδ1(τ) distance. The simulated REDOR curves in Fig. 2A already took into account the 30% presence of the π-tautomer, which contributed a Cα-Nε2 distance of 4.38 Å for $\chi_2 = 180^\circ$, 4.52 Å for $\chi_2 = -60^\circ$, and 4.59 Å for $\chi_2 = +60^\circ$.

For the pH 4.5 sample, the Nδ1 and Nε2 peaks overlap at ~178 ppm (Fig. S1A), thus the Cα signal was simultaneously dephased by Nδ1 and Nε2. The REDOR curve fitting thus required a three-spin geometry, with a fixed 25° angle between the Cα-Nδ1 and Cα-Nε2 vectors. The three-spin simulation was carried out in SIMPSON (*13*). For each χ_2, the relative Cα-Nδ1 and Cα-Nε2 distances are fixed. For $\chi_2 = 180^\circ$ (*t*), the Cα-Nδ1 distance is 3.9 Å while the Cα-Nε2 distance is 4.4 Å. For $\chi_2 = -60^\circ$ (*m*), the Cα-Nδ1 distance is 3.2 Å while the Cα-Nε2 distance is 4.5 Å. For $\chi_2=+60^\circ$ (*p*), the Cα-Nδ1 distance is 3.2 Å while the Cα-Nε2 distance is 4.6 Å.

To fit the Cδ2-Nα REDOR data for extracting χ_1, no lipid natural abundance correction was necessary, since the Cδ2 signal did not overlap with any lipid signals. The His37 Nα signal was also well resolved from all other ^{15}N signals.

Extraction of motionally averaged sidechain $^{13}C\{^{15}N\}$ dipolar couplings

At pH 4.5, the high-temperature Cγ-{Nδ1, Nε2} REDOR data was analyzed in a three-spin geometry similar to the low-temperature distance analysis described above. The data mainly reflects the Cγ-Nδ1 order parameter, because the two-bond Cγ-Nε2 dipolar coupling is much weaker, with a rigid-limit value of only 285 Hz. Moreover the Cγ-Nε2 vector is roughly parallel

to the Cβ-Cγ motional axis, thus Cγ-Nε2 coupling is insensitive to χ_2 torsional dynamics. Therefore, we held the Cγ-Nε2 coupling fixed at 285 Hz while varying the Cγ-Nδ1 coupling to fit the REDOR data. The resulting Cγ-Nδ1 coupling was 980 Hz, indicating a motional order parameter of 0.85.

In these Cγ-detected REDOR experiments, the S/S_0 values decreased to ~0.4 instead of 0 due to the presence of natural abundance lipid ^{13}C intensities.

Calculation of order parameters for various two-site jump motions

In the motionally averaged tensor (also called the sum tensor) shown in Figure S7A, the three principal axes (red, Σ_i, I = 1, 2, 3) are oriented as follows: one principal axis is along the bisector of the Z_A and Z_B vectors, a second principal axis is perpendicular to the plane of the Z_A and Z_B vectors, and the third principal axis is perpendicular to the other two principal axes. Designating the directional angles between the three averaged principal axes and either bond as Θ_n, the principal values of the motionally averaged tensor are:

$$\bar{\omega}_n = \frac{1}{2}\delta\left(3\cos^2\Theta_n - 1\right) \qquad (1)$$

Once the principal values are obtained, the motionally averaged anisotropy parameter $\bar{\delta}$ is calculated as the difference from the isotropic value of the principal value that is furthest away from the isotropic value. The ratio between the averaged anisotropy parameter and the rigid-limit δ is the order parameter *S*, $S \equiv \bar{\delta}/\delta$.

The relation between the torsional angle change $\Delta\chi$ around a motional axis and the reorientation angle β of a bond is

$$\sin\frac{\beta}{2} = \sin\frac{\Delta\chi}{2}\cdot\sin\theta, \qquad (2)$$

where θ is the angle between the motional axis and the bond of interest. The directional angles are related to β as: $\Theta_{1,2} = 90^\circ - \beta/2$, $\Theta_{2,1} = \beta/2$, and $\Theta_3 = 90^\circ$.

As an example, we consider 180° flips of the imidazole ring around the Cβ-Cγ bond, $\Delta\chi_2 = 180^\circ$. The reorientation angle is then $\beta = 2\theta$, since $\sin\frac{\beta}{2} = \sin 90^\circ \sin\theta = \sin\theta$. For the Cγ-Nδ1 bond, $\theta = 57^\circ$ with respect to the Cβ-Cγ bond, so $\beta = 114^\circ$. As a result, $\Theta_1 = 33^\circ$, $\Theta_2 = 57^\circ$, and $\Theta_3 = 90^\circ$. The motionally averaged principal values are thus:

$$\begin{aligned} \bar{\omega}_1 &= \tfrac{1}{2}\delta\left(3\cos^2 33^\circ - 1\right) = 0.56\delta \\ \bar{\omega}_2 &= \tfrac{1}{2}\delta\left(3\cos^2 57^\circ - 1\right) = -0.06\delta, \\ \bar{\omega}_3 &= \tfrac{1}{2}\delta\left(3\cos^2 90^\circ - 1\right) = -0.5\delta \end{aligned} \qquad (3)$$

The motionally averaged anisotropy parameter is $\bar{\delta} = \bar{\omega}_1 = 0.56\delta$, which gives a Cγ-Nδ1 order parameter of $S_{CN} \equiv \bar{\delta}/\delta = 0.56$ for 180° ring flips.

For 180° χ_1 angle changes around the Cα-Cβ axis while χ_2 is fixed at 180°, since the Cγ-Nδ1 bond is only 8.2° from the Cα-Cβ bond, $\beta = 16^\circ$. Thus the motionally averaged principal values are $\bar{\omega}_1 = 0.97\delta$, $\bar{\omega}_2 = -0.47\delta$, and $\bar{\omega}_3 = -0.5\delta$. This means the Cγ-Nδ1 order parameter is 0.97 for 180° χ_1 changes, which is much higher than the measured order parameter of 0.85. Figure S7 similarly shows that no χ_1 change can satisfy the measured Cδ2-Hδ2 order parameter of 0.80. Therefore, the experimentally measured order parameters rule out χ_1 changes as a possible motional mechanism.

Proposed model of ring-flip assisted proton conduction by M2

Liposome assays (*14*) showed that the M2 proton conductance increased by ~14 fold from 18°C to 37°C. This temperature dependence indicates that the total energy barrier for proton conductance is ~104 kJ/mol:

$$\frac{G_{H+,310K}}{G_{H+,291\,K}} = e^{\frac{-E_{a,}}{R}\cdot\left(\frac{1}{310}-\frac{1}{291}\right)} \approx 14 \quad \Rightarrow E_a \approx 104\ kJ/mol. \qquad (4)$$

This energy barrier is consistent with the barrier for histidine sidechain motion (> 59 kJ/mol) obtained from NMR dipolar couplings at pH 4.5 to 6. But it does not agree with the calculated energy barrier (29-42 kJ/mol) for proton hopping through the charged His37 tetrad, which is the rate-limiting step in the shutter model. Thus, the similar temperature dependences of proton conductivity and His37 sidechain motion suggest the shuttle model for proton conduction by M2. Specifically, we propose that proton conduction is achieved by His37 ring-flip-mediated proton dissociation and association. Below we qualitatively outline the energetic aspects of this model.

The imidazolium reorientation rate observed by NMR dipolar couplings is on the order of $5 \times 10^4\ s^{-1}$ (**Fig. S8**). On the other hand, the value of single-channel proton conductance of M2 has significant uncertainty and varies with the experimental method and condition. In two recent authoritative studies, one study concluded a single-channel current of ~0.5 fA at pH 6.2 (*15*), while the other study measured a value of 2.7 aA at 18°C and pH 5.7 (*14*). Based on the unitary current of the first study, a proton dissociation rate constant, k_{H+}, of $\sim 1.7 \times 10^4\ s^{-1}$ was obtained (*15*), which is very close to the imidazolium ring flip rate. Since a basic unit of the proton conduction cycle **(Fig. 4E)** includes both ring motions and the proton transfer reaction, the similarity of k_{H+} and the sidechain motional rate means that proton transfer is extremely fast, with a negligible energy barrier.

The second study reported much lower conductance values (*14*), which at 37°C were about 250 H^+/s per channel (*14*). Since at pH 5.7 the number of imidazoliums per channel is about 3 (*16*), the conductance per imidazolium is $k_{H+} \approx 250/3 = 83/s$. This rate constant is 100-1000 times smaller than the ring-flip rate, which suggests that the proton transfer reaction may be much slower than in the first estimate above. Based on the Arrhenius equation, the ratio of 100-1000 translates to an energy barrier of 12-18 kJ/mol for proton transfer, which is still much lower than the barrier of imidazolium motion. Thus, even using the lower limit of proton conductance functional data, the highest energy barrier of proton conduction is still the barrier for imidazolium motion.

This ring-motion-assisted proton transfer model is consistent with the observed deuterium isotope effect of M2 (*15*), where H^+ are conducted 1.8 – 2.5 times faster than D^+ by M2. This ratio is significantly larger than if water diffusion is the mechanism (predicted ratio = 1.25), and also larger than if the H^+ and D^+ mobility in the respective solvent (H_2O and D_2O) is the mechanism (predicted ratio = 1.4-1.5) (*17*). Instead, the magnitude of the isotope effect suggests

proton dissociation in a mixed hydrogen-bonded chain with dissimilar elements, which supports the current model. The 2-fold difference in H^+ and D^+ conductance may be explained by an increased energy barrier of ~1.7 kJ/mol for D^+ dissociation than H^+ dissociation.

Analysis of Cε1-Hε1 bond length from low-temperature dipolar couplings

To obtain the His37 Cε1-Hε1 bond length at low temperature, we considered the contribution of lipid intensities to the Cε1 peak at 134 ppm. The sphingomyelin C5 peak resonates at 134 ppm and at 243 K cannot be resolved from the Cε1 peak (*18*). Based on the protein/lipid molar ratio and the 1.1% natural abundance of ^{13}C, this SPM C5 intensity is only 6% of the labeled Cε1 peak intensity. Approximating that the SPM C5 peak has comparable C-H dipolar coupling as the main lipid CH_2 peak at 32 ppm, we obtained the CH_2 coupling strength, and used it to simulate the expected SPM C5-H dipolar dephasing curve. We then fitted the total intensities including the lipid effect according to the relative intensities of the two spins. The resulting C-H bond length is 1.20 Å for the pH 8.5 sample and 1.19 Å for the pH 4.5 sample, which are within ±0.02 Å of the values without the lipid natural abundance correction (Fig. 4B).

These Cε1-Hε1 bond lengths are unusually long (weak dipolar couplings). Due to the high signal/noise ratio, where the error bars are smaller than the data symbols in Fig. 4B, the random uncertainties were at most ±0.4 kHz in the dipolar couplings or ±0.02 Å in the distances. There are three possible sources of systematic uncertainty: 1) uncertainty in the ^1H homonuclear decoupling scaling factor, 2) residual motion, and 3) the contribution of lipid natural abundance signals (discussed above). The first two sources were internally calibrated and largely excluded by the Cδ2-Hδ2 coupling measured in the same experiment, at the same temperature and under identical homonuclear decoupling. The Cδ2-Hδ2 coupling reached the rigid limit of 23.9 kHz, indicating the absence of motion and an unstretched bond length of 1.08 Å. Thus, the homonuclear decoupling scaling factor did not bias the couplings to smaller values. The possibility of long-range effects from protons in the rest of the imidazole ring can also be ruled out because additional protons can only increase the coupling, not decrease it. Therefore, the weak Cε1-Hε1 coupling at both pH values cannot be attributed to experimental uncertainty, and can only be attributed to bond stretching.

N-H bond lengths in hydrogen-bonded imidazole model compounds have been measured by McDermott and coworkers and found to be stretched from 1.01 Å to as long as 1.07 Å (*19*). For O-H…O systems, much longer O-H bond stretching by as much as 0.3 Å was known. In comparison, C-H bond stretching in hydrogen bonds has been much less explored. The weak coupling may be due to proton hopping or partial occupancy of the proton at Cε1, or due to true stretching of the covalent bond that results from an altered potential well for Hε1. The former scenario is unlikely because we did not observe any temperature dependence of the ^{13}C and ^{15}N chemical shifts, which would be expected for proton hopping. Therefore, the most reasonable interpretation of the weak Cε1-Hε1 dipolar coupling is stretching of the covalent bond by hydrogen bonding. Indeed, a recent *ab initio* study of various types of hydrogen bonding in aromatic amino acids, including Phe, Tyr, Trp and His, found that the Cε1-H bond of imidazole rings experience the strongest C-H…O hydrogen bonding and the largest bond elongation (*20*). This effect was attributed to the acid nature of the Cε1-H group between two nitrogens. Thus, the computation result was qualitatively consistent with the observed bond stretching here. The exact magnitude of the Cε1 bond stretching awaits future investigation and experimental confirmation.

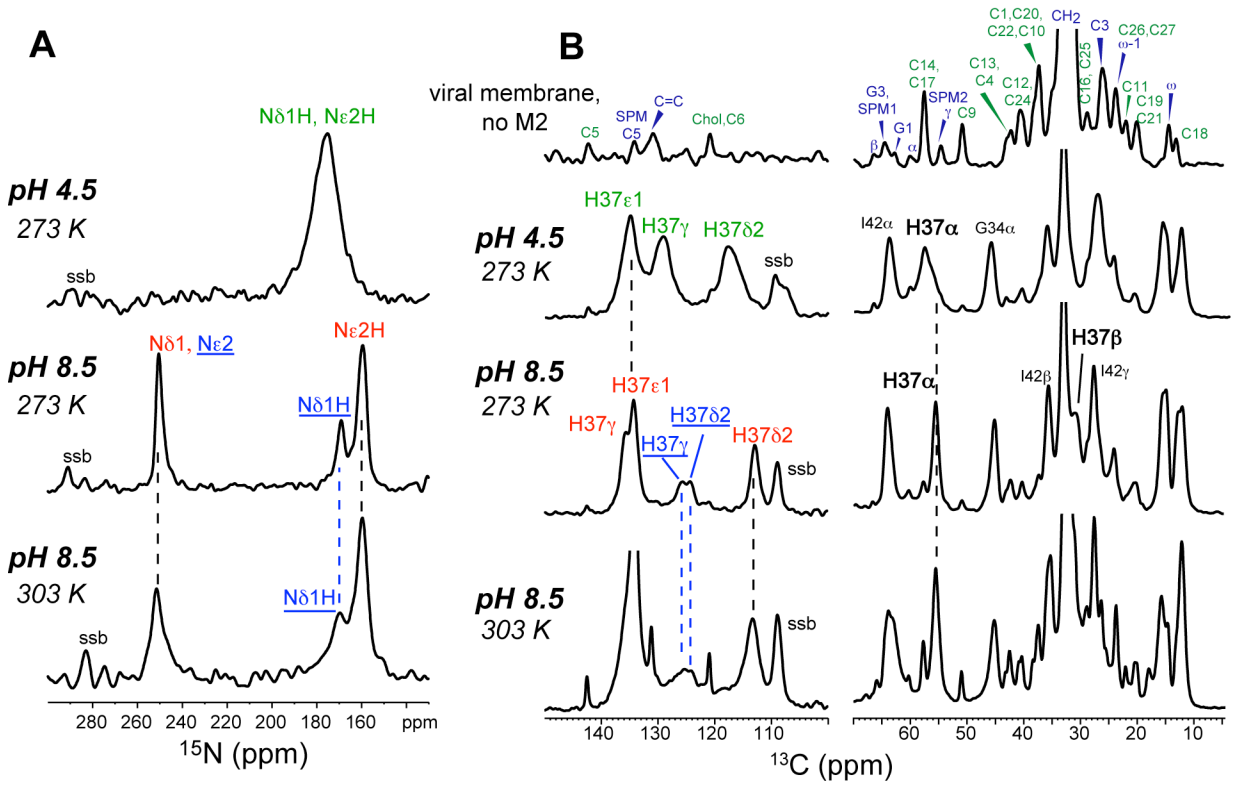

Figure S1. 1D ^{13}C and ^{15}N MAS spectra of His37-labeled M2TM at pH 8.5 and 4.5 at indicated temperatures. **(A)** ^{15}N CP-MAS spectra. The ^{1}H-^{15}N CP contact time was 3 ms at 273 K and 1.5 ms at 303 K. The CP matching condition was optimized using ^{15}N-tBoc-proline to ensure maximal transfer of the ^{1}H magnetization to unprotonated ^{15}N. Thus, the lack of ~250 ppm ^{15}N peak in the pH 4.5 spectrum indicates virtually no (≤5%) neutral imidazoles at pH 4.5, which translates to a fourth pKa of ~ 4.7 for the His37 tetrad, consistent with previous estimates in model membranes (*16*). At pH 8.5, the π-tautomer signals were resolved from the τ-tautomer signals at both 273 K and 303 K, indicating no exchange between the two tautomers. The imidazole peaks were assigned in red for the neutral τ-tautomer, in blue for the neutral π-tautomer, and in green for the charged histidine. **(B)** ^{13}C CP-MAS spectra of the virus-mimetic lipid membrane without the protein (top), the membrane-bound M2TM at pH 4.5 at 273 K, and at pH 8.5 at 273 K and 303 K. In the lipid-only spectrum, blue designates sphingomyelin (SPM), DPPC and DPPE peaks, and green denotes cholesterol peaks (*1*). The two neutral tautomers were observed at both temperatures in the pH 8.5 spectra, confirming slow or no exchange.

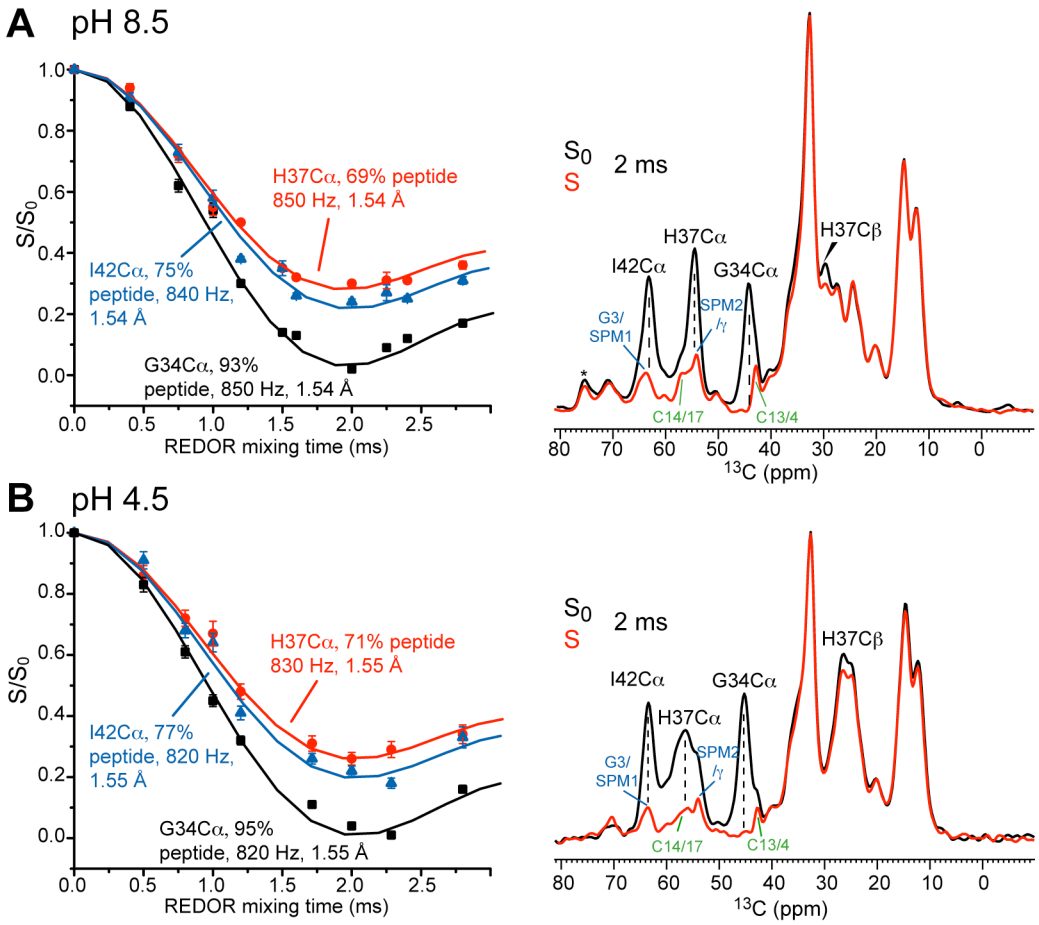

Figure S2. One-bond Cα–Nα REDOR data of M2TM to determine the percentage of lipid ^{13}C intensities that overlaps with the His37 Cα peak. This information was necessary for quantifying the Cα–Nδ1 distance in Fig. 2 to determine the χ_2 torsion angle. The experiment did not involve frequency-selective ^{15}N irradiation since sidechain nitrogens are too far from Cα to affect the one-bond dipolar coupling. **(A)** pH 8.5. **(B)** pH 4.5. All REDOR curves show rigid-limit Cα-Nα dipolar couplings consistent with the bond length, which is expected for the protein at the experimental temperature of 233 K. The minimum S/S_0 value indicates the amount of lipid natural abundance ^{13}C intensities that overlap with the protein Cα peaks. Representative REDOR control (S_0, black) and dephased (S, black) spectra are shown on the right. The lipid peaks are labeled in green for cholesterol and blue for SPM, DPPC and DPPE. The REDOR experiments were carried out at several spinning speeds (5-8 kHz for pH 8.5 and 4-7 kHz for pH 4.5) in order to densely sample the mixing times.

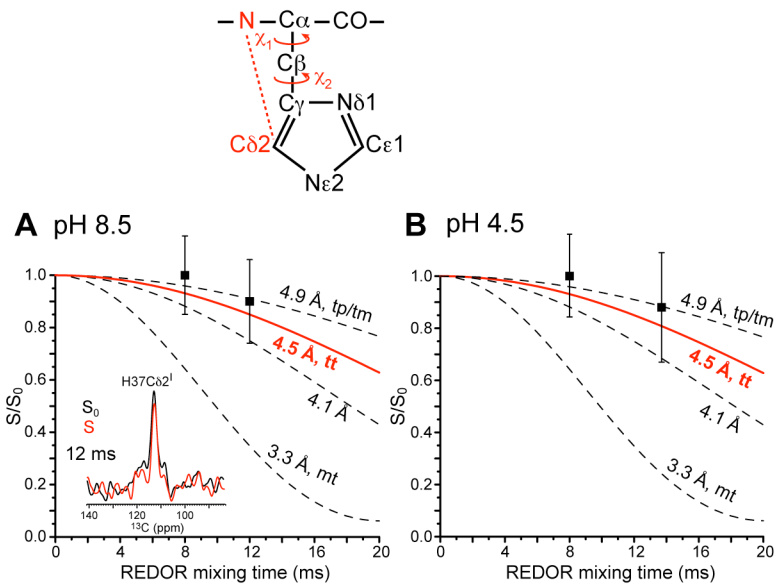

Figure S3. Cδ2-Nα REDOR distance data to constrain the His37 rotameric conformation. Representative $^{13}C\{^{15}N\}$ selective REDOR spectra are shown. S_0: control spectrum (black). S: dephased spectrum (red). **(A)** pH 8.5. **(B)** pH 4.5. Both samples exhibit Cδ2-Nα distances of 4.5 – 4.9 Å, indicating that the χ_1 angle is 180° (*t*), given the χ_2 angle of 180° obtained from Cα-Nδ1 distances (Fig. 2). A χ_1 of -60° combined with a χ_2 of 180° would give a much shorter distance (3.3 Å) that is inconsistent with the data. The χ_1=+60° rotamer is not allowed in α-helices due to steric conflict with the backbone (*21*). Rotamer notations: *t*: 180°, *p*: +60°, and *m*: -60°. The REDOR experiments were carried out at 233 K under 7-8 kHz MAS.

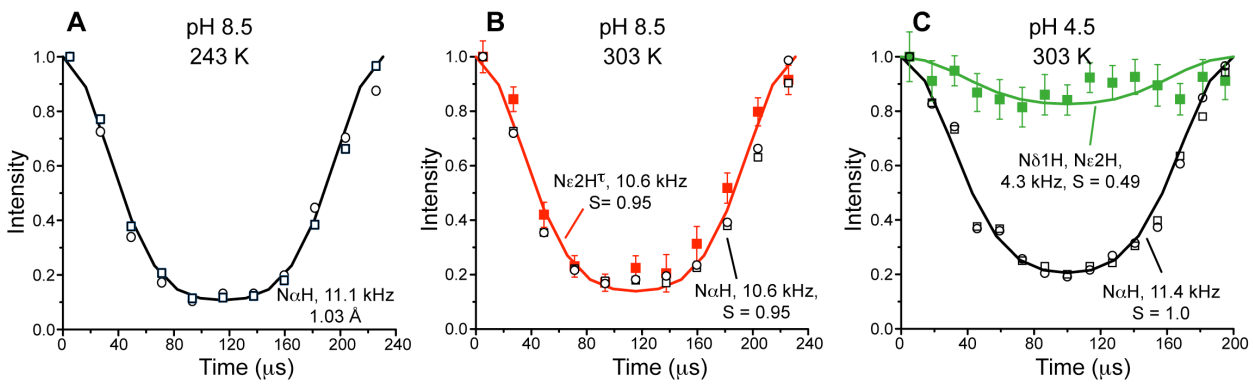

Figure S4. ^{15}N-^{1}H dipolar couplings of His37 in M2TM to determine bond lengths at low temperature and sidechain dynamics at high temperature. **(A)** 243 K N-H coupling of backbone amide at pH 8.5 corresponds to a bond length of 1.03 Å. **(B)** 303 K N-H dipolar couplings at pH 8.5. Both the backbone amide and the sidechain Nε2(τ) show close to rigid-limit couplings. The former confirms immobilization of the M2 backbone by the viral membrane at physiological temperature, while the latter indicates the absence of sidechain motion in the closed channel at physiological temperature. **(C)** 303 K N-H dipolar couplings at pH 4.5. The backbone Nα-Hα coupling remains in the rigid limit, while the sidechain Nδ1 and Nε2 exhibit much weaker N-H couplings, indicating sidechain motion. The order parameter of 0.49 was obtained by dividing the measured coupling with the low-temperature value of 8.8 kHz (Fig. 4A). This low order parameter results from the combined effect of sidechain motion and hydrogen exchange between NH and water protons. The DIPSHIFT experiments were carried out under 4.3 kHz MAS for the pH 8.5 sample and 5 kHz MAS for the pH 4.5 sample.

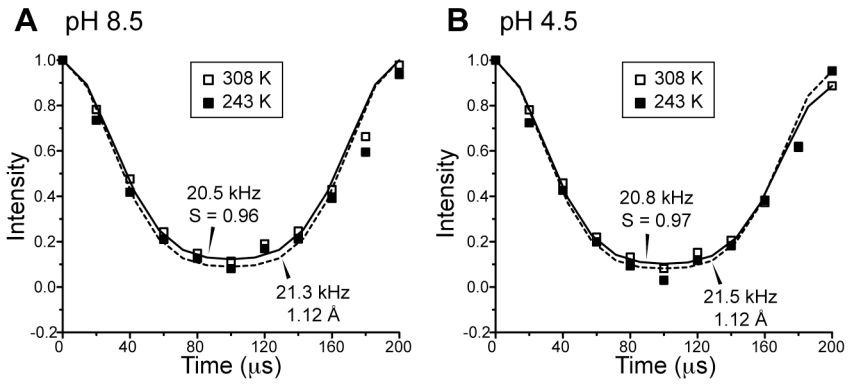

Figure S5. His37 Cα-Hα dipolar couplings at 308 K confirm immobilization of the M2 backbone in the cholesterol-containing viral membrane at physiological temperature. **(A)** pH 8.5. **(B)** pH 4.5. The 308 K couplings approach the rigid limit and are close to the low-temperature (243 K) values at both pH. The experiments were carried out under 5 kHz MAS.

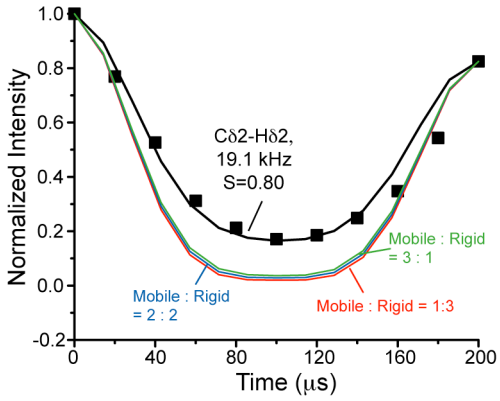

Figure S6. Predicted dipolar couplings and order parameters for heterogeneous His37 sidechain motion. Calculated Cδ2-Hδ2 dipolar couplings are shown for cases where one to three imidazoliums in each channel undergoes 180˚ ring flips while the others are immobilized. The calculated dephasing curves are all much lower than the experimental data, thus ruling out heterogeneous ring flips. The mobile : immobile ratios are 3:1 for the green curve, 2:2 for the blue curve, and 1:3 for the red curve.

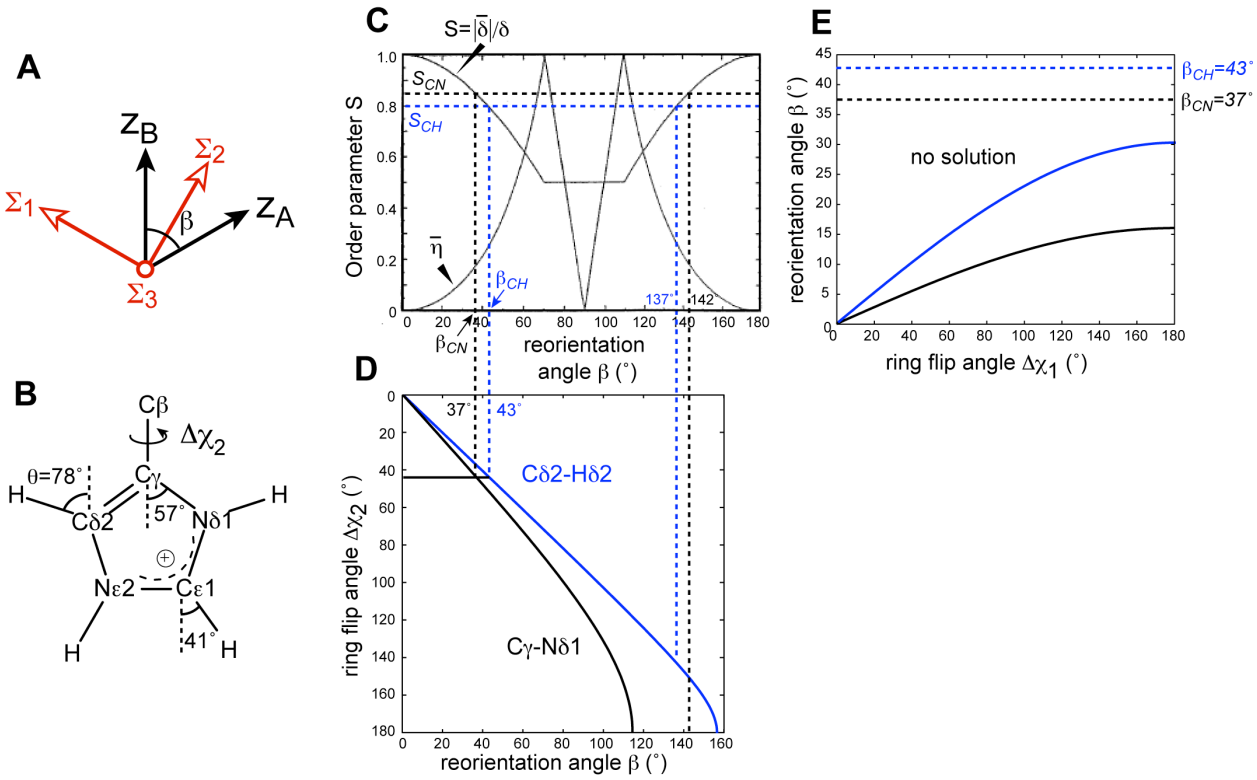

Figure S7. Calculation of order parameters for two-site jumps of imidazolium rings at low pH. **(A)** General geometry of two-site jumps, where a bond reorients by an angle β between Z_A and Z_B. The orientations of the averaged principal axis system (Σ_1, Σ_2, Σ_3) are indicated in red. **(B)** Geometry of the imidazolium, where the angles θ between several bonds and the Cβ-Cγ axis are indicated. **(C)** Dependence of the motional order parameter $S=|\bar{\delta}|/\delta$ on the reorientation angle β for two-site jumps, adapted from (*22*). The measured order parameter values for Cγ-Nδ1 (0.85) and Cδ2-Hδ2 (0.80) bonds are indicated as dashed lines. Two β solutions, centered at 40° and 140°, are found. **(D)** Relation between the reorientation angle β and the ring flip angle $\Delta\chi_2$. Both Cδ2-Hδ2 and Cγ-Nδ1 order parameters are satisfied only at a single $\Delta\chi_2$ of ~45°. The other β solution of 140° cannot be satisfied because no χ_2 changes can reorient the Cγ-Nδ1 bond by more than 114°. **(E)** Relation between β and χ_1 changes. No χ_1 changes can satisfy the experimental constraint of β= 40° or 140°, since both Cγ-Nδ1 and Cδ2-Hδ2 bonds are approximately parallel to the Cα-Cβ bond under a trans χ_2 angle. In other words, ring reorientation around the Cα-Cβ bond will cause little changes in the Cγ-Nδ1 and Cδ2-Hδ2 bond orientations, and thus will cause very little reduction of these couplings.

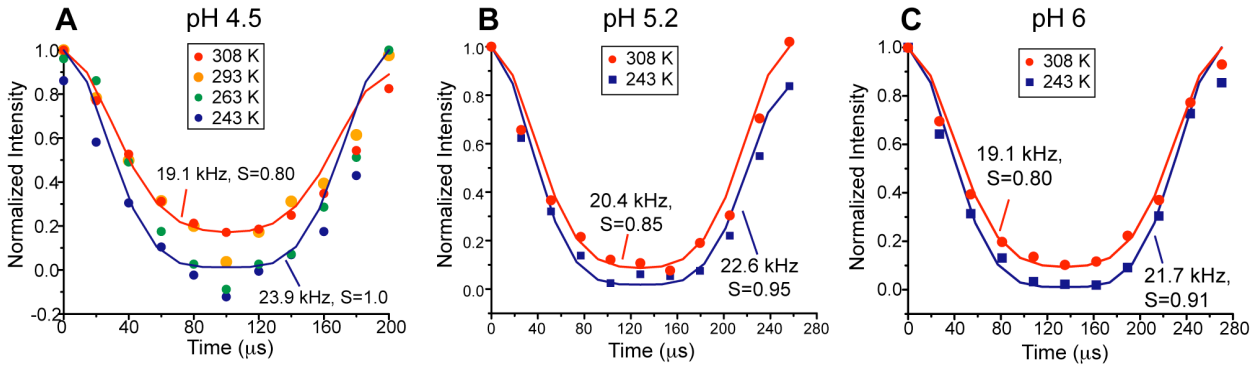

Figure S8. His37 sidechain motion at pH 4.5, pH 5.2 and pH 6.0 at physiological temperature. Cδ2-Hδ2 dipolar coupling was measured at 243 K to confirm the rigid limit and at 308 K to obtain dynamics information. **(A)** pH 4.5 data at 308 K, 293 K, 263 K, and 243 K. The coupling was scaled by an order parameter of 0.80 at both 308 K and 293 K, indicating that the imidazolium motion was in the fast limit. At 263 K the coupling reached the rigid limit, indicating the ring motion was frozen. At 273 K an intermediate order parameter of 0.92 was found (not shown). **(B)** pH 5.2 data at 308 K and 243 K, extracted from the charged Cδ2 chemical shift of 117.6 ppm. **(C)** pH 6.0 data at 308 K and 243 K, extracted from the neutral Cδ2 chemical shift of 113 ppm. For both pH 5.2 and pH 6, the high-temperature order parameters are similar to what is measured at pH 4.5, thus His37 sidechain motion occurs not only at pH 4.5 but also at the physiological pH of the virus. The similar sidechain mobility in the less charged His37 tetrad at pH 6 also suggests that motion is an intrinsic property of a spacious conducting channel, rather than a direct function of the charged state of His37.

For a motional process to cause fast averaging of an interaction, the motional rate has to be significantly larger than the coupling of interest. Likewise, for a slow motion to not induce intermediate-timescale line broadening, the motional rate k must be significantly smaller than the coupling of interest. For an FSLG-scaled ^{13}C-^{1}H rigid-limit coupling of ~13 kHz, we used a factor of 4 for the lower-bound and upper bound, thus giving $R_{flip,293\,K} \geq 52\ kHz$ and $R_{flip,263\,K} \leq 3.3\ kHz$. Thus, at pH 4.5, the lower limit of the activation energy of the motion is:

$$\frac{R_{flip,293\,K}}{R_{flip,263\,K}} = e^{-\frac{E_a}{R}\left(\frac{1}{293}-\frac{1}{263}\right)} \geq 16 \Rightarrow E_a \geq 59\ kJ/mol$$

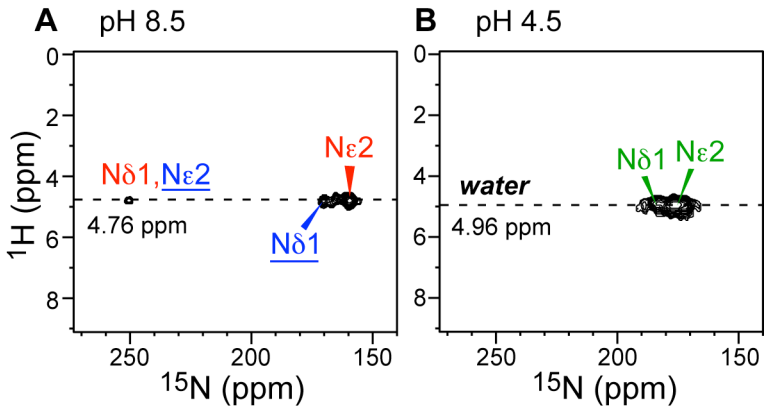

Figure S9. 2D water-His37 ^{1}H-^{15}N correlation spectra of M2TM in viral membranes. **(A)** pH 8.5. **(B)** pH 4.5. The spectra were measured at 303 K under 4.5 and 4.0 kHz MAS. A 1 ms ^{1}H-^{15}N HH-CP contact time and a 50 μs ^{1}H spin diffusion mixing time were used to transfer the water polarization to His37. Since the ^{1}H-^{1}H homonuclear dipolar coupling is scaled by -0.5 during HH-CP, the total effective ^{1}H spin diffusion mixing time was 0.55 ms, which was much shorter than the length of 4 ms used to show the near absence of water-G34 cross peak in amantadine-bound and dehydrated M2TM channels (*18*). Thus, the presence of imidazole-water cross peaks at both pH indicates the presence of water near His37. In particular, at high pH, a weak water cross peak with the unprotonated Nδ1 was detected, indicating that the C-terminus of His37 was not completely devoid of water.

Table S1. Full widths at half maximum (ppm) of His37 sidechains at pH 8.5 and pH 4.5, measured at 273 K [a].

Site	pH 8.5	pH 4.5
Cγ	2.5	3.0
Cδ2	2.0	4.0
Nδ1	3.5[b]	8.4
Nε2	5.4[b]	7.0

[a]. The linewidths were obtained from resolved peaks in 1D or 2D spectra, with identical line broadening parameters of LB = -15 and GB = 0.04.

[b]. These linewidths refer to the major τ-tautomer.

Table S2. Bond order parameters for different motional models of the imidazole ring around the Cβ-Cγ bond.

Bonds	S_{exp}	180° ring flip		45° ring flip		Uniaxial rotation	
		β	S	β	S	Cone angle	S
Cγ-Nδ1	0.85	114°	0.56	37°	0.85	57°	-0.06
Cδ2-Hδ2	0.80	156°	0.94	43°	0.80	78°	-0.44
Cε1-Hε1	0.95	82°	0.50	28°	0.91	41°	0.35

References

1. W. Luo, S. D. Cady, M. Hong, *Biochemistry* **48**, 6361 (2009).
2. S. D. Cady, M. Hong, *J. Biomol. NMR* **45**, 185 (2009).
3. S. D. Cady, M. Hong, *Proc. Natl. Acad. Sci. U.S.A* **105**, 1483 (2008).
4. K. Takegoshi, S. Nakamura, T. Terao, *Chem. Phys. Lett.* **344**, 631 (2001).
5. M. Hong, R. G. Griffin, *J. Am. Chem. Soc.* **120**, 7113 (1998).
6. M. G. Munowitz, R. G. Griffin, G. Bodenhausen, T. H. Huang, *J. Am. Chem. Soc.* **103**, 2529 (1981).
7. A. Bielecki, A. C. Kolbert, M. H. Levitt, *Chem. Phys. Lett.* **155**, 341 (1989).
8. W.-K. Rhim, D. D. Elleman, R. W. Vaughan, *J. Chem. Phys.* **59**, 3740 (1973).
9. M. Hong *et al.*, *J. Magn. Reson.* **129**, 85 (1997).
10. C. M. Rienstra *et al.*, *Proc. Natl. Acad. Sci. USA* **99**, 10260 (2002).
11. C. P. Jaroniec, B. A. Tounge, J. Herzfeld, R. G. Griffin, *J. Am. Chem. Soc.* **123**, 3507 (2001).
12. N. Sinha, K. Schmidt-Rohr, M. Hong, *J. Magn. Reson.* **168**, 358 (2004).
13. M. Bak, T. Rasmussen, N. C. Nielsen, *J. Magn. Reson.* **147**, 296 (2000).
14. T. I. Lin, C. Schroeder, *J. Virol.* **75**, 3647 (2001).
15. J. A. Mould *et al.*, *J. Biol. Chem.* **275**, 8592 (2000).
16. J. Hu *et al.*, *Proc. Natl. Acad. Sci. U.S.A.* **103**, 6865 (2006).
17. T. E. DeCoursey, V. V. Cherny, *J. Gen. Physiol.* **109**, 415 (1997).
18. W. Luo, M. Hong, *J. Am. Chem. Soc.* **132**, 2378 (2010).
19. X. J. Song, C. M. Rienstra, A. E. McDermott, *Magn. Reson. Chem.* **39**, S30 (2001).
20. S. Scheiner, T. Kar, J. Pattanayak, *J. Am. Chem. Soc.* **124**, 13257 (2002).
21. S. C. Lovell, J. M. Word, J. S. Richardson, D. C. Richardson, *Proteins: Struct., Funct., Genet.* **40**, (2000).
22. K. Schmidt-Rohr, H. W. Spiess, *Multidimensional Solid-State NMR and Polymers*. (Academic Press, San Diego, 1994), pp. 478.